Investigating effect on contact stiffness on the Low Velocity Impact Response of Curved Composite Plate

BUDDHI ARAHCHIGE, HESSAM GHASEMNEJAD, ANDRE AGOUSTI
School of Aerospace and Aircraft Engineering
Kingston University
Friars Avenue, London, SW15 3DW
UNITED KINGDOM
Buddhi.Arahchige@kingston.ac.uk

Abstract: - The low velocity impact response of a curved stiffness composite panel is studied. A two degree of freedom spring-mass model is used to evaluate the contact force between the composite panel and the impactor. This work uses the Hertzian contact model which is linearized for the impact analysis of the curved composite panel. First order shear deformation theory coupled with Fourier series is used to derive the governing equations of the curved composite panel. In this paper, the effect of contact stiffness on the impact force is studied analytically. The results showed that the impact force increased with increase of contact stiffness.

Key-Words: - FSDT, CPT, Hertzian, MATLAB, stiffness matrix

1 Introduction

Composites are been widely used in various engineering fields since it has many advantages such as been lightweight, have high stiffness to weight ratios, good fatigue performance and excellent corrosion resistance. The major automotive industries are also utilizing composites to assist them meet the performance and weight requirements. For high performance Formula 1 racing cars, most of the components such as chassis, monocoque, suspension and engine cover is manufactured from composites. [1]. However these advantages are slightly restrained by their high susceptibility to internal damage caused by foreign object damage. The impact process damages the structure and reduces its useful life. The failure modes of composite structures are different from metals. There are two main mechanisms of damage in composites. They are intra-laminar damage mechanisms (resin or fibre dominated failures due to tensile, compressive or out of plane stresses) and inter-laminar damage, which is delamination. [2]

Interface delaminations are usually the most critical failure mechanisms since they severely degrade the strength and the integrity of the structure. These failure modes under low velocity impact depends upon the fibre type, resin type, lay-up, thickness, and projectile type.

The use of Charpy tests, drop towers have been used in impact testing of composites. Various researchers have studied the impact behaviour of composite laminates. Several types of mathematical models have been built in order to study this impact behaviour.

Gong *et al*. [3] studied the elastic response of orthotropic laminated cylindrical shells to low-velocity impact. A spring-mass model was developed to determine the contact force between the shell and the impactor. An analytical function for the contact force was derived in terms of material properties and the mass of the shell and the impactor, as well as for the impact velocity. Khalili [4] studied the dynamic response of thin smart curved composite panel subjected to low-velocity transverse impact. First order shear deformation was used to obtain the structural field.

Martinez *et. al.* [5] performed impact tests over a carbon fibre reinforced epoxy using low energy in the striker. A non-conservative and nonlinear spring-clashpot series model was proposed to reproduce the material behaviour. The model considered simultaneously both flexural and indentation

phenomena accounting for energy losses by means of the restitution coefficient. This model enabled the accurate prediction of the contact force duration.

Hassan et al. [6] addressed the response of Glass Fiber Reinforced Plastic laminates (GFRPs) under low-velocity impact. Experimental tests were performed according to ASTM: D5628 for different initial impact energy levels ranging from 9.8 J to 29.4 J and specimen thicknesses of 2, 3 and 4 mm. The impact damage process and contact stiffness were studied incrementally until a perforation phase of the layered compounds occurred, in line with a force–deflection diagram and imaging of impacted laminates. The effect that impact parameters such as velocity and initial energy had on deflection and damage of the test specimens was explored.

Ghasemnejad *et al* [7] studied the Charpy impact behaviour of single and multi-delaminated hybrid composite beam structures. The Charpy impact test was chosen to study the energy absorption capability of delaminated composite beam. It was shown that the composite beams with closer position of delamination to impacted surface are able to absorb more energy in comparison with other delamination positions in hybrid and non-hybrid ones.

Krishnamurthy *et al* [8] studied the impact response of a laminated composite cylindrical shell determined both by the classical Fourier series and the finite element methods. Impact response determined by the finite element method also includes a prediction of the impact-induced damage deploying the semi-empirical damage prediction model of Choi–Chang. The parametric carried out by the finite element method investigated the effect of governing parameters such as impactor mass, its approach velocity, curvature of the shell, on both the impact response and on the impact-induced damage.

Ghasemnejad *et al* [9] studied the damage behavior of naturally stitched composite single lap joints under low velocity impact. In order to study the energy absorbing capability, Charpy Impact tests were used. It was proved that the composite beams stitched through the thickness were able to absorb more energy in comparison with adhesively bonded composite joints.

Caputo *et al* [10] proposed numerical techniques to describe the damage initiation and propagation of impact damages in composite structures. An explicit finite element analysis was developed through utilizing a global/local finite element model and the model predicted the propagation of both interlaminar and intralaminar damages.

Laminated theories have been widely used to study and predict the impact damage of composite structures. These theories can be classified as equivalent single layer (ESL), layer-wise and zig-zag theories. The ESL theories can be divided into three main categories: classical plate theory (CPT), first-order shear deformation theory (FSDT) and higher order shear deformation theories (HSDTs). Shear deformation effects are ignored by the CPT and it provides reasonable results for thin laminates. Nonetheless, it underestimates the deflection and overestimates the buckling load and frequency of thick laminates where shear deformation effects are more distinct. Shear deformation effects are accounted through the FSDT proposed by Reissner [11] and Mindlin [12] by the way of linear variation of in-plane displacements through the thickness. A shear correction factor is essential to compensate for the difference between actual stress state and presumed constant stress state since the FSDT violates the equilibrium conditions on the top and bottom surfaces of the plate. [13]. This paper makes use of the FSDT to predict the impact response of the composite plate.

There are several factors affecting impact damage. It is vital to identify the material properties that have an effect on impact damage as it would assist in designing improved materials and impact resistance composites. Improved impact resistance is obtained through using high strain to failure fibers, tougher resins and stitched laminates. The elastic properties of the material (E_1, E_2, v_{12}, G_{12}) along with the lamination orientation, define the overall rigidities of the plate which largely affect the contact force history. Experiments with the same matrix material and five different types of fiber reinforcements demonstrated an equal threshold damage energy, indicating that the damage initiation was matrix-dominated. The stacking sequence and the properties of the reinforcing fibers had no major effect on the energy required for damage initiation.

Damage is initiated by matrix cracking and when a matrix crack reaches an interface between layers with different fiber orientations, delamination is initiated [14]. The target stiffness also have a significant effect on the contact force history. At low velocities, flexible targets respond primarily by bending, which causes high tensile stresses in the lowest ply. Matrix cracks then developed in the lowest ply, which in turn generated a delamination at the lowest interface. This

matrix cracking-delamination repeats itself from ply to ply resulting in an inverted pine tree appearance. For stiffer targets, damage is initiated by high contact stresses and propagates downwards through the same matrix cracking-delamination process. Another factor affecting impact damage is the properties of the impactor, its size and shape, the material it is made of and the angle of incidence relative to the surface of the specimen. [14].

2 Problem Formulation

2.1 Theoretical Analysis

Love's equations of motion for a cylindrical shell of length L, radius R and thickness h subjected to external loads are expressed as:

$$\frac{\partial N_x}{\partial x}+\frac{1}{R}\frac{\partial N_{x\theta}}{\partial \theta}+q_x(x,\theta,t)=\rho h\ddot{u} \quad (1)$$

$$\frac{\partial N_{x\theta}}{\partial x}+\frac{1}{R}\frac{\partial N_\theta}{\partial \theta}+\frac{Q_\theta}{R}+q_\theta(x,\theta,t)=\rho h\ddot{v} \quad (2)$$

$$\frac{\partial Q_x}{\partial x}+\frac{1}{R}\frac{\partial Q_\theta}{\partial \theta}-\frac{N_\theta}{R}+q_n(x,\theta,t)=\rho h\ddot{w} \quad (3)$$

$$\frac{\partial M_x}{\partial x}+\frac{1}{R}\frac{\partial M_{x\theta}}{\partial \theta}-Q_x=\frac{\rho h^3}{12}\ddot{\beta}_x \quad (4)$$

$$\frac{\partial M_{x\theta}}{\partial x}+\frac{1}{R}\frac{\partial M_\theta}{\partial \theta}-Q_\theta=\frac{\rho h^3}{12}\ddot{\beta}_\theta \quad (5)$$

The constitutive equations of a specially orthotropic material are described as:

$$\begin{Bmatrix} N_x \\ N_\theta \\ N_{x\theta} \end{Bmatrix}=\begin{bmatrix} A_{11} & A_{12} & 0 \\ A_{12} & A_{22} & 0 \\ 0 & 0 & A_{66} \end{bmatrix}\begin{Bmatrix} \varepsilon_x^0 \\ \varepsilon_\theta^0 \\ \gamma_{x\theta}^0 \end{Bmatrix} \quad (6)$$

$$\begin{Bmatrix} M_x \\ M_\theta \\ M_{x\theta} \end{Bmatrix}=\begin{bmatrix} D_{11} & D_{12} & 0 \\ D_{12} & D_{22} & 0 \\ 0 & 0 & D_{66} \end{bmatrix}\begin{Bmatrix} \kappa_x \\ \kappa_\theta \\ \kappa_{x\theta} \end{Bmatrix} \quad (7)$$

$$\begin{Bmatrix} Q_x \\ Q_\theta \end{Bmatrix}=\begin{bmatrix} kA_{55} & 0 \\ 0 & kA_{44} \end{bmatrix}\begin{Bmatrix} \gamma_{xz}^0 \\ \gamma_{\theta z}^0 \end{Bmatrix} \quad (8)$$

Where

$$\{A_{ij},D_{ij}\}=\int_{-h/2}^{h/2}\bar{Q}_{ij}(1,z^2)dz \quad \text{(i, j = 1,2,6)} \quad (9)$$

$$A_{ii}=\int_{-h/2}^{h/2}\bar{C}_{ii}dz \quad \text{(i,i =4, 5)} \quad (10)$$

$\bar{Q}_{ij}$ are the transformed reduced stiffnesses in the $x-\theta$ plane, $\bar{C}_{ii}$ are the transformed shear stiffnesses, and k is the Mindlin shear correction factor which is $\pi^2/12$. [12]

The strain-displacement relations are expressed as:

$$\varepsilon_z^0=\frac{\partial u}{\partial x} \quad \varepsilon_\theta^0=\frac{1}{R}\frac{\partial v}{\partial \theta}+\frac{w}{R} \quad \gamma_{x\theta}^0=\frac{\partial u}{\partial x}+\frac{1}{R}\frac{\partial u}{\partial \theta}$$

$$\kappa_x=\frac{\partial \beta_x}{\partial x} \quad \kappa_\theta=\frac{1}{R}\frac{\partial \beta_\theta}{\partial \theta} \quad \kappa_{x\theta}=\frac{\partial \beta_0}{\partial x}+\frac{1}{R}\frac{\partial \beta_x}{\partial \theta} \quad (11)$$

$$\gamma_{xz}^0=\beta_x+\frac{\partial w}{\partial x} \quad \gamma_{\theta z}^0=\beta_\theta+\frac{1}{R}\frac{\partial w}{\partial \theta}-\frac{v}{R}$$

The solution to the dynamic problem is based on the expansion of the loads, displacement, and rotations functions in double Fourier series. Double Fourier series, for the displacements and the rotation of rectangular doubly curved composite panel with simply supported boundary conditions are defined according to [4]:

$$u_0(x_1,x_2,t)=\sum_{n=1}^{\infty}\sum_{m=1}^{\infty}U_{mn}(t)cos\frac{m\pi x_1}{a}sin\frac{n\pi x_2}{b} \quad (12)$$

$$u_0(x_1,x_2,t)=\sum_{n=1}^{\infty}\sum_{m=1}^{\infty}V_{mn}(t)sin\frac{m\pi x_1}{a}sin\frac{n\pi x_2}{b} \quad (13)$$

$$w_0(x_1,x_2,t)=\sum_{n=1}^{\infty}\sum_{m=1}^{\infty}W_{mn}(t)sin\frac{m\pi x_1}{a}sin\frac{n\pi x_2}{b} \quad (14)$$

$$\varphi_1(x_1,x_2,t)=\sum_{n=1}^{\infty}\sum_{m=1}^{\infty}X_{mn}(t)cos\frac{m\pi x_1}{a}sin\frac{n\pi x_2}{b} \quad (15)$$

$$\varphi_2(x_1,x_2,t)=\sum_{n=1}^{\infty}\sum_{m=1}^{\infty}Y_{mn}(t)sin\frac{m\pi x_1}{a}sin\frac{n\pi x_2}{b} \quad (16)$$

For a concentrated load located at the point,

$$Q_{mn}(t)=\frac{4F(t)}{ab}sin\frac{m\pi x_1^c}{b};\ m,n=1,3,5,\ldots$$

$$\begin{bmatrix} c_{11} & c_{12} & c_{13} & c_{14} & c_{15} \\ c_{12} & c_{22} & c_{23} & c_{24} & c_{25} \\ c_{13} & c_{23} & c_{33} & c_{34} & c_{35} \\ c_{14} & c_{24} & c_{34} & c_{44} & c_{45} \\ c_{15} & c_{25} & c_{35} & c_{45} & c_{55} \end{bmatrix} \begin{Bmatrix} U_{mn}(t) \\ V_{mn}(t) \\ W_{mn}(t) \\ X_{mn}(t) \\ Y_{mn}(t) \end{Bmatrix} = \begin{Bmatrix} 0 \\ 0 \\ \rho h \ddot{W}_{mn}(t) - Q_{mn}(t) \\ 0 \\ 0 \end{Bmatrix} \quad (17)$$

$$U_{mn}(t) = K_U W_{mn}(t) \quad (18)$$

$$V_{mn}(t) = K_V W_{mn}(t) \quad (19)$$

$$X_{mn}(t) = K_X W_{mn}(t) \quad (20)$$

$$Y_{mn}(t) = K_Y W_{mn}(t) \quad (21)$$

Where:

$$K_U = S_1 + S_2 K_X + S_3 K_Y \quad (22)$$

$$K_V = S_4 + S_5 K_X + S_6 K_Y \quad (23)$$

$$K_X = \Delta_X / \Delta \quad (24)$$

$$K_Y = \Delta_Y / \Delta \quad (25)$$

$$\Delta_X = (c_{35} + c_{15}s_1 + c_{25}s_4)(c_{45} + c_{14}s_3 + c_{24}s_6) - (c_{34} + c_{14}s_1 + c_{24}s_6)(c_{55} + c_{15}s_3 + c_{25}s_6) \quad (26)$$

$$\Delta_Y = (c_{45} + c_{15}s_2 + c_{25}s_5)(c_{34} + c_{14}s_1 + c_{24}s_4) - (c_{44} + c_{14}s_2 + c_{24}s_5)(c_{35} + c_{15}s_1 + c_{25}s_4) \quad (27)$$

$$\Delta = (c_{44} + c_{14}s_2 + c_{24}s_5)(c_{55} + c_{15}s_3 + c_{25}s_6) - (c_{45} + c_{14}s_3 + c_{24}s_6)(c_{45} + c_{15}s_2 + c_{25}s_5) \quad (28)$$

Where:

$$s_1 = \frac{c_{12}c_{23} - c_{22}c_{13}}{s} \quad (29)$$

$$s_2 = \frac{c_{12}c_{24} - c_{22}c_{14}}{s} \quad (30)$$

$$s_3 = \frac{c_{12}c_{25} - c_{22}c_{15}}{s} \quad (31)$$

$$s_4 = \frac{c_{12}c_{13} - c_{11}c_{23}}{s} \quad (32)$$

$$s_5 = \frac{c_{12}c_{14} - c_{11}c_{24}}{s} \quad (33)$$

$$s_6 = \frac{c_{12}c_{15} - c_{11}c_{25}}{s} \quad (34)$$

$$s = c_{11}c_{22} - c_{12}^2 \quad (35)$$

The operators of c_{ij} are evaluated as [4]:

$$c_{11} = -A_{11}\left(\frac{m^2\pi^2}{a^2}\right) - A_{66}\left(\frac{n^2\pi^2}{b^2}\right) - \left(\frac{k_{sh}}{R_1^2}\right)A_{55} \quad (36)$$

$$c_{12} = -\left(\frac{m\pi}{a}\right)\left(\frac{n\pi}{b}\right)(A_{12} + A_{66}) \quad (37)$$

$$c_{13} = \frac{1}{R_1}\left(\frac{m\pi}{a}\right)A_{11} + \frac{1}{R_2}\left(\frac{m\pi}{a}\right)A_{12} + \frac{k_{sh}}{R_1}\left(\frac{m\pi}{a}\right)A_{55} \quad (38)$$

$$c_{14} = -\left(\frac{n^2\pi^2}{b^2}\right)c_0 D_{66} + \frac{k_{sh}}{R_1}A_{55} \quad (39)$$

$$c_{15} = -\left(\frac{m\pi}{a}\right)\left(\frac{n\pi}{b}\right)c_0 D_{66} \quad (40)$$

$$c_{22} = -\left(\frac{n^2\pi^2}{b^2}\right)A_{22} - \frac{k_{sh}}{R_2^2}A_{44} - \left(\frac{m^2\pi^2}{a^2}\right)A_{66} \quad (41)$$

$$c_{23} = \frac{1}{R_1}\left(\frac{m\pi}{b}\right)A_{12} + \frac{1}{R_2}\left(\frac{n\pi}{b}\right)A_{22} + \frac{k_{sh}}{R_1}\left(\frac{n\pi}{b}\right)A_{44} \quad (42)$$

$$c_{24} = \left(\frac{m\pi}{a}\right)\left(\frac{n\pi}{b}\right)c_0 D_{66} \quad (43)$$

$$c_{25} = \frac{k_{sh}}{R_2}A_{44} + \left(\frac{m^2\pi^2}{a^2}\right)c_0 D_{66} \quad (44)$$

$$c_{33} = -k_{sh}\left(\frac{m^2\pi^2}{a^2}\right)A_{55} - k_{sh}\left(\frac{n^2\pi^2}{b^2}\right)A_{44} - \left(\frac{1}{R_2^2}\right)A_{22} - \left(\frac{1}{R_1^2}\right)A_{11} \quad (45)$$

$$c_{35} = -k_{sh}\left(\frac{m\pi}{a}\right)A_{55} \quad (46)$$

$$c_{35} = -k_{sh}\left(\frac{n\pi}{b}\right)A_{44} \quad (47)$$

$$c_{44} = -\left(\frac{m^2\pi^2}{a^2}\right)D_{11} - \left(\frac{n^2\pi^2}{b^2}\right)D_{66} - k_{sh}A_{55} \quad (48)$$

$$c_{45} = -\left(\frac{m^2\pi^2}{a^2}\right)D_{12} - \left(\frac{m\pi}{a}\right)\left(\frac{n\pi}{b}\right)D_{66} \quad (49)$$

$$c_{55} = -\left(\frac{m^2\pi^2}{a^2}\right)D_{66} - \left(\frac{n^2\pi^2}{b^2}\right)D_{22} - k_{sh}A_{44} \quad (50)$$

$$\ddot{W}_{mn}(t) + \omega_{mn}^2(t) = \frac{Q_{mn}(t)}{\rho h} \quad (51)$$

The natural frequency of the plate is calculated by;

$$\omega_{mn}^2 = \frac{-(c_{13}K_U + c_{23}K_V + c_{33} + c_{34}K_X + c_{35}K_Y)}{\rho h} \quad (52)$$

$$W_{mn}(t) + \omega_{mn}^2 W_{mn}(t) = \frac{4F(t)}{ab\rho h} sin\frac{m\pi x_1^c}{a} sin\frac{n\pi x_2^c}{b} \quad (53)$$

For zero initial displacement and velocity of the panel, the solution becomes:

$$W_{mn}(t) = \frac{1}{\omega_{mn}}\frac{4}{ab\rho h} sin\frac{m\pi x_1^c}{a} sin\frac{n\pi x_2^c}{b}\int_0^t F(\tau)\, sin\omega_{mn}(t-\tau)d\tau$$
(54)

2.2 Impact Model

In the existing S-M model, M_1 and M_2 represent the mass of the shell and the impactor respectively; K_1 is the stiffness constant of the shell and K_2 is the stiffness constant of the impactor. The stiffness of the simply supported laminated shell can be defined as:

$$K_1 = \omega_1^2 M_1 \quad (40)$$

Where ω_1 is the fundamental frequency of the laminated shell and obtained through equation (37) by applying $m = n = 1$.

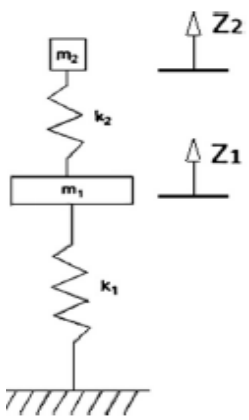

Fig. 1 A two degree of freedom spring-mass model [2]

If $z_1(t)$ represent the radial displacement of the load point of the shell and $z_2(t)$ represent that of the impactor at any time t during the impact, then the contact deformation is expressed as:

$$\partial(t) = z_2(t) - z_1(t) \quad (55)$$

It is assumed that the Hertzian theory governs the contact force between the impactor and the laminated shell during the impact and is given by:

$$F_c(t) = K_2(\partial^p) \quad (56)$$

Where K_2 and p are material constants obtained through static indentation tests [3].
Deriving an analytical solution for the contact force is a challenging task as the equation (56) is non-linear. Therefore, the existing approach employs an effective contact stiffness K_2^* in order to relate the equivalent contact force to the contact deformation.

$$F_c^*(t) = K_2^*\partial \quad (57)$$

Which can also be expressed as,

$$F_c^*(t) = K_2^*[z_2(t) - z_1(t)] \quad (58)$$

The effective contact stiffness K_2^* is expressed as:

$$K_2^* = \sqrt{\pi}\Gamma\left(\frac{p+1}{2}\right)\frac{2\Gamma\left(\frac{p}{2}+1\right)+\sqrt{\pi}\Gamma\left(\frac{p+1}{2}\right)}{4\Gamma^2\left(\frac{p}{2}+1\right)+\pi\Gamma^2\left(\frac{p+1}{2}\right)}\delta_m^{p-1}K_2 \quad (59)$$

Where Γ is the Gamma function and the maximum contact deformation, ∂_m is given by:

For a target with free edges [1]:

$$\partial_m = \left(\frac{M_1M_2}{M_1+M_2}\right)^{0.4}\left[\frac{5V^2}{4k_2}\right]^{0.4} \quad (60)$$

For a target with clamped edges [1]:

$$\partial_m = (M_2)^{0.4}\left[\frac{5V^2}{4k_2}\right]^{0.4} \quad (61)$$

This study involves a target structure with simply supported edges and ∂_m for simply supported target structure is expressed as:

$$(\partial_m)_f < (\partial_m)_{ss} < (\partial_m)_c \quad (62)$$

Where the subscripts f, ss, c refer to free, simply supported and clamped respectively.

The corresponding equations of motion for a two degree of freedom model is as follows [2]:

$$m_1\ddot{z_1} = -k_1z_1 - k_2(z_1 - z_2) \quad (63)$$

$$m_2\ddot{z_2} = -k_2(z_2 - z_1) \quad (64)$$

The initial conditions are defined as:

$$z_1 = z_1 = z_2 = 0, \quad z_2 = V \quad at\ t = 0 \quad (65)$$

By using the initial conditions defined in equation (51), the analytical function for the force can be defined as:

$$F_c^*(t) = K_2^*[A_1(C_1 - 1)sin\omega_1 t + A_2(C_2 - 1)sin\omega_2 t] \quad (66)$$

The coefficients in the analytical function for the force are derived as: [2]

$$\omega_{1,2}^2 = \frac{1}{2}\left(\frac{k_1+k_2}{M_1} + \frac{k_2}{M_2}\right) \mp \sqrt{\frac{1}{4}\left(\frac{k_1+k_2}{M_1} + \frac{k_2}{M_2}\right)^2 - \frac{k_1 k_2}{M_1 M_2}}$$
(67)

$$C_1 = \frac{k_2}{k_2 - \omega_1^2 M_2} \quad (68)$$

$$C_2 = \frac{k_2}{k_2 - \omega_2^2 M_2} \quad (69)$$

$$A_1 = \frac{V}{\omega_1(C_1 - C_2)} \quad (70)$$

$$A_1 = \frac{V}{\omega_2(C_2 - C_1)} \quad (71)$$

3 Problem Solution

Calculations based on the present analysis were performed for impact on 48-ply laminate open cylindrical shells consisting a $[(\pm 45/0_2)_2/\pm 45/0/90]_{2s}$ lay-up fabricated from graphite/epoxy prepreg. The dimensions of the shell analyzed in this study are identical to the studies carried out by Gong et.al [ ]. The shell has a radius of 0.0254m, a length of 0.6096m, a width of 0.2032m and a thickness of 0.0127. The geometrical and material properties of the composite panel are shown in Table [ ]. The values of ∂_m, K_2 and p are calculated to be $10^{-4}m$, $120 \times 10^8 Nm^{-1.5}$ and 1.5. K_2^* was determined from equation [59] and the mass M_2 was 3kg. A generic MATLAB script was written in order to calculate the stiffness matrices and the equivalent contact force.

E_{11}	141.2GPa
$E_{22}=E_{33}$	9.72GPa
$G_{12}=G_{13}$	5.53GPa
G_{23}	3.74GPa
$v_{12}=v_{13}=v_{23}$	0.30
ρ	$1536kg/m^3$

Table 1 Material properties of the laminated composite shell

E	207GPa
V	0.30
ρ	$7800kg/m^3$
Tip diameter	20mm
Mass of the impactor	3kg
Impactor velocity	6m/s

Table 2 Material properties of the impactor

$A_{11}(Nm^{-1})$	1.04×10^9	$D_{11}(Nm)$	1.41×10^4
$A_{12}(Nm^{-1})$	2.33×10^8	$D_{12}(Nm)$	3.45×10^3
$A_{22}(Nm^{-1})$	4.86×10^8	$D_{22}(Nm)$	5.77×10^3
$A_{33}(Nm^{-1})$	2.66×10^8	$D_{66}(Nm)$	3.89×10^3
$A_{44}(Nm^{-1})$	6.99×10^8	$D_{11}(Nm)$	1.41×10^4
$A_{55}(Nm^{-1})$	6.99×10^8	M_1 (kg)	0.95

Table 3 Stiffness matrix values

3.1 Contact Force History plots

The contact force histories are plotted to investigate the effect of the contact stiffness on the contact force. In the first instance, the steel plate was simulated to vailidate the equations. Figure 2 shows the impact results for the steel plate when compared with the results derived by Gong et.al [1] and Khalili [2].

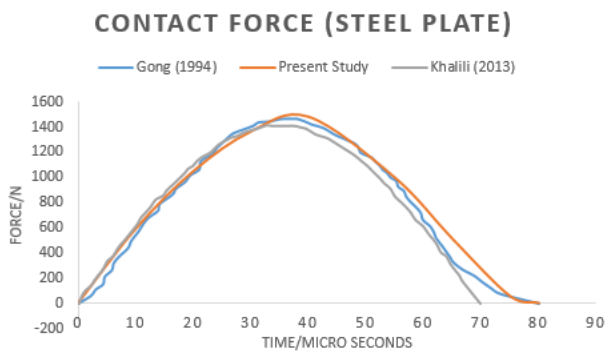

Fig. 2 Contact Force History (Steel Plate)

The above results showed that the maximum contact force for the present study was higher compared to the past studies carried out by Gong et.al [1] and Khali [2]. This was due to the fact that the current study yielded a higher contact stiffness, k_2 than the earlier anlysis.

3.2 Effect on contact stiffness, k_2 on contact force

The main aim of this paper was to study the effect of the contact stiffness on the contact history. Figure 3 shows the contact force history based on the calculated value of k_2 which is $120 \times 10^8 Nm^{-1.5}$

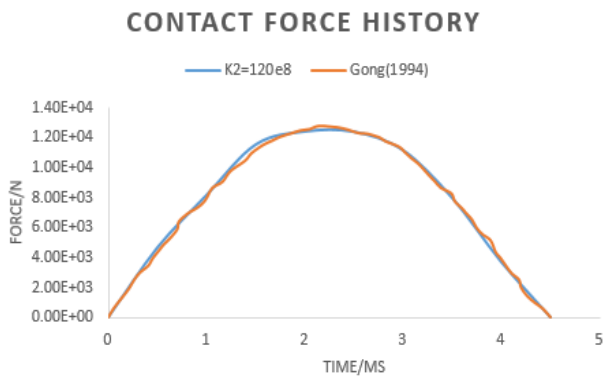

Fig. 3 Contact force vs time (k_2=$120 \times 10^8 \mathrm{Nm}^{-1.5}$)

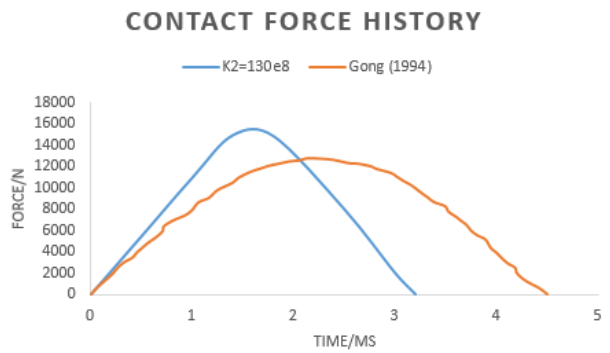

Fig. 4 Contact force vs time (k_2=$130 \times 10^8 \mathrm{Nm}^{-1.5}$)

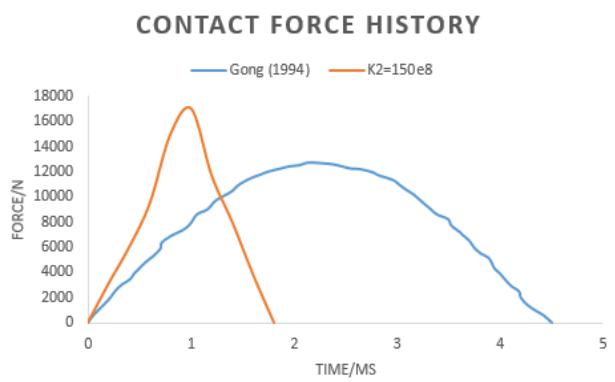

Fig. 5 Contact force vs time (k_2=$150 \times 10^8 \mathrm{Nm}^{-1.5}$)

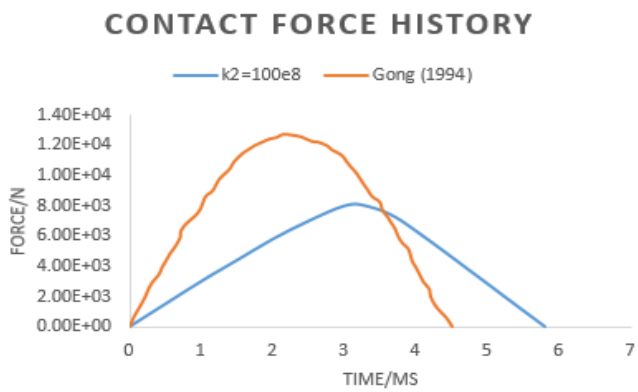

Fig 6 Contact force vs time (k_2=$100 \times 10^8 \mathrm{Nm}^{-1.5}$)

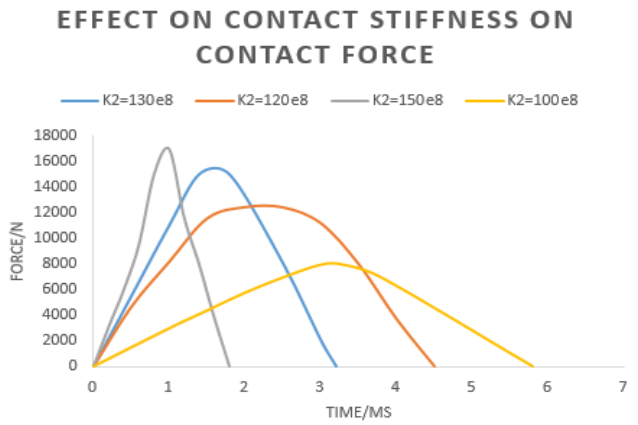

Fig. 7 Contact force vs time (combined)

It can be seen from the above analysis that the contact force increases with increase of the contact stiffness, k_2, but the contact duration decreases. The higher k2 yields to a higher effective contact stiffness, K_2^*. Therefore, the higher the contact stiffness between the shell and the impactor, the more spontaneous the contact force. This means that a larger force is acting over a shorter time period. Likewise, more higher modes of vibration are generated due to the shorter contact time as the impact by a stiffer impactor is more spontaneous.

4 Conclusion

This paper evaluated the effect on the contact stiffness on the contact force history. A two degree of freedom spring-mass model facilitated the use of a pre-derived analytical force function consisting of several material parameters. This contact force function was utilized to analyze the contact force between the impactor and the target shell structure

during the impact and study the complete contact force history.

References:

[1] Campbell, F. (2010). Introduction to Composite Materials. Structural Composite Materials 2010; pp.4-18.

[2] Tiwari, N. Introduction to Composite Material and Structures. Failure of Composites 2000; Kanpur, India: India Institute of Technology.

[3] Gong SW, Toh SL, Shim VPW. The elastic response of orthotropic laminated cylindrical shells to low-velocity impact. Compos Eng 1994; 4:241-66.

[4] Khalili SMR, Ardali A. Low velocity impact response of doubly curved symmetric cross-ply laminated panel with embedded SMA wires. Composite Structures 2013; pp.216-226.

[5] Martinez AB, Sanchez-Soto M, Velasco JI, Maspoch MLI, Santana OO, Gordillo A. Impact characterization of a carbon fiber-epoxy laminate using a nonconservative model. J Appl Polym Sci, Vol 97, 2005, pp. 2256–63.

[6] Hassan MA, Naderi S, Bushroa AR. Low velocity impact damage of woven fabric composites: Finite Element simulation and experimental verification. Materials and Design, Vol 53, 2014, pp. 706-718.

[7] Ghasemnejad H, Furquan ASM, Mason PJ. Charpy Impact damage behavior of single and multi-delaminated hybrid composite beam structures. Materials and Design, Vol 31, 2010, pp.3653-3660.

[8] Krishnamurthy, K. S., P. Mahajan, et al. (2003). "Impact Response and Damage in Laminated Composite Cylindrical Shells." Composite Structures Vol 59(1), pp. 15-36.

[9] Ghasemnejad H, Argentiero Y, Tez TA, Barrington PE. Impact damage response of natural stitched single lap-joint in composite structures. Materials and Design, Vol 51, 2013, pp.552-560

[10] Caputo F, Luca De A, Lamanna G, Borrelli R, Mercurio U. Numerical study for the structural analysis of composite laminates subjected to low velocity impact, Composites: Part B, Vol 67, 2014, pp. 296-302.

[11] Reissner E. The effect of transverse shear deformation on the bending of elastic plates. Journal of Applied Mechanics, Vol.12, 1945, pp. 69-72

[12] Mindlin RD, Influence of rotary inertia and shear on flexural motions of isotropic elastic plates, Journal of Applied Mechanics, Vol.18, 1951, pp. 31-8.

[13] Thai TH, Choi HD, A simple first-order shear deformation theory for laminated composite plates, Composite Structures, Vol.106, 2013, pp.754-763.

[14] Abrate S, Modelling of Impact on composite structures, Composite Structures, Vol.51, 2001, pp. 129-38